ADVANCED FUNCTIONAL MATERIALS
www.afm-journal.de

Spontaneous Current Oscillations during Hard Anodization of Aluminum under Potentiostatic Conditions

By *Woo Lee,* Jae-Cheon Kim,* and *Ulrich Gösele*

Nanoporous anodic aluminum oxide is prepared by hard anodization of aluminum under potentiostatic conditions using 0.3 M $H_2C_2O_4$. Under unstirred electrolyte condition, spontaneous current oscillations are observed. The amplitude and period of these current oscillations are observed to increase with anodization time. As a consequence of the oscillatory behavior, the resulting anodic alumina exhibits modulated pore structures, in which the diameter contrast and the length of pore modulation increase with the amplitude and the period of current oscillations, respectively, and the current peak profile determines the internal geometry of oxide nanopores. The mechanism responsible for the oscillatory behavior is suggested to be a diffusion-controlled anodic oxidation of aluminum.

1. Introduction

Over the past six decades, anodization processes have intensively been utilized in the aluminum industry for diverse applications such as electronics, architecture, packaging, and transport.[1] A typical anodization process involves electrochemical oxidation of aluminum under a galvanostatic or potentiostatic condition using an appropriate acid electrolyte (e.g., sulfuric, oxalic, or phosphoric acid) in order to form porous anodic aluminum oxide (AAO) film that is conformally in contact with the underlying metal. The morphology of AAO consists of hexagonal arrays of straight long cylindrical nanopores oriented perpendicular to the metal/oxide interface, where each pore is closed by a thin barrier oxide layer with hemispherical geometry.[2] Based on recent research progress in developing long-range ordered pore structures, the anodization process has attracted considerable interest in the use of the resulting AAO as template for fabricating low-dimensional nanostructures over a macroscopic area, overcoming many of the drawbacks of conventional lithographic techniques.[3–10]

AAO membranes with tailor-made internal pore structure could provide not only a new degree of freedom in template-based fabrications of advanced functional materials, but also a model system for investigating separations of particles and adsorption characteristics of molecules.[11–13] Recently, we have realized the fabrication of AAO membranes with periodically modulated diameter of nanopores by combining conventional mild anodization (MA) at low current density ($j = 1$–5 mA cm^{-2}) and a newly developed hard anodization (HA) process at high current density ($j = 30$–250 mA cm^{-2}), in which each modulation step required the exchange of the electrolyte solutions in order to satisfy both MA and HA processing conditions.[14] Following the work, we were able to develop a process called ''pulse anodization'', which allows continuous engineering of both internal pore structure and composition of nanoporous AAO avoiding the tedious periodic replacement of the electrolyte solutions.[15,16] Periodic pulses consisting of a low potential (or galvanic) pulse followed by a high potential (or galvanic) pulse were applied to achieve MA and HA conditions, respectively. In an attempt to improve our previous works, more recently Losic et al. have developed a process termed ''cyclic anodization (CA)'', in which the anodizing current in the form of periodic waves was applied in order to combine MA and HA conditions.[17] Although they demonstrated successful transformation of the current profiles into structural pore features, pores are often distorted losing their directional coherency.

In this article we report spontaneous oscillations of current during potentiostatic HA of aluminum under specific electrochemical conditions and their effect on the internal pore structure of the resulting anodic aluminum oxide (AAO). We found that AAOs that experienced oscillatory kinetic behavior exhibit modulated pore structures, in which the modulation patterns follow exactly the details of the oscillating current profile. In our earlier investigations on HA of aluminum in sulfuric acid under galvanostatic conditions, oscillating pore diameters were also observed experimentally but an association with voltage oscillations was not observed and no detailed explanation of this behavior could be found although an association with the development of gas bubbles was suggested.[18] To the best of our knowledge, therefore, this is the first detailed report regarding self-induced oscillatory kinetic behavior during anodization of aluminum. For anodic oxidations of semiconductors, there have been a number of reports of oscillatory behaviors during the anodization of silicon and III-V compound semiconductors (e.g., n-InP, GaAs), and

[*] Dr. W. Lee, J.-C. Kim
Korea Research Institute of Standards and Science
Yuseong, 305-340 Daejon (Korea)
E-mail: woolee@kriss.re.kr
Prof. U. Gösele
Max Planck Institute of Microstructure Physics
Weinberg 2, 06210 Halle (Germany)

DOI: 10.1002/adfm.200901213

attempts have been made to understand the observed oscillatory behaviors also theoretically.[19–28] On the other hand, there have been few reported cases of oscillatory behavior for anodic oxidation of valve metals, although quite recently Taveira et al. reported voltage oscillations during galvanostatic anodization of Ti.[29] Here, we discuss a possible origin of self-induced oscillatory kinetic behaviors during HA of aluminum and the effect of current oscillations on the morphology of the resulting AAO and compare with other known cases in anodic oxidations of silicon and titanium. Due to the highly ordered nature of modulated pores, it is expected that anodic alumina membranes can readily be utilized as templates for fabricating novel nanowires or nanotubes, whose diameters are periodically modulated along their axes, and thus, enable one to study topography-induced optical, electronic, and magnetic properties.

2. Results and Discussion

2.1. Current Oscillations versus Internal Pore Structure

Recently, we have reported that current during HA of aluminum decreases almost exponentially as a function of time,[14,15,18,30] unlike the case of conventional mild anodizations (MA), in which current density (j) is maintained at a steady-state value throughout anodization.[31] Such a current–time transient for HA has been attributed to the diffusion-limited electrochemical oxidation of aluminum at the pore base as a consequence of fast growth of anodic oxide over the whole sample area.[14] In other words, since the anodization current is mainly related to the movement of ionic species (OH^-, O^{2-}, Al^{3+}) through the barrier oxide at the bottom of pores, the mass transport of oxygen-containing anionic species from the bulk electrolyte to the reaction interface (i.e., oxide/metal interface) determines the current during the anodization process. Thus, the ionic current is expected to gradually decrease over time due to the extended diffusion path along the nanopores, resulting in a non-linear growth rate of anodic films. In the present study, the first-step HA that was performed under a previously established condition (i.e., $U_1 = 140$ V, vigorously stirred 0.3 M $H_2C_2O_4$ at 0 °C) exhibited a typical current–time transient observed in HA consistently with our previous report (see Fig. S1, Supporting Information).[14] On the other hand, an intriguing evolution of current was observed during the second-step HA that was carried out at an anodization voltage ranging from $U_2 = 140$ V to 200 V with an unstirred electrolyte at an elevated temperature of aluminum substrate (i.e., 5 °C), as we will discuss in detail below.

Figure 1a shows a representative current (j)–time (t) transient during the second-step HA at $U_2 = 160$ V, together with enlarged current profiles of the early and later stage of the anodization as insets. As evident from the present j–t curve, the current oscillates spontaneously. The peak values ($j_{Max} \approx 0.7$ A cm^{-2}) of current are roughly one order and two orders of magnitude higher than those of standard $H_2C_2O_4$-based HA and MA, respectively.[14] Upon close examination, one can find the following three features from the j–t curve: i) The period of oscillations increases with the anodization time (t). ii) The amplitude (A) increases with time (t) at the early stage of anodization but stabilizes to an almost steady-state value at the later stage. iii) The current profile of the early stage

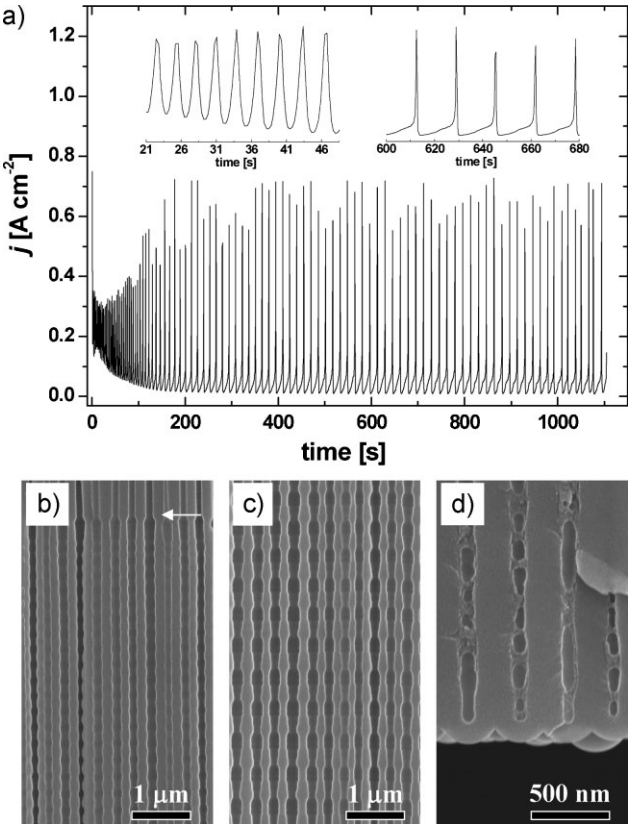

Figure 1. a) Current (j)–time (t) transient during the second-step HA at 160 V using 0.3 M $H_2C_2O_4$ at the substrate (Al) temperature of 5 °C, showing oscillatory kinetics of aluminum anodization. The enlarged j–t curves at the early and later stage of anodization are presented as inset. b–d) Cross-sectional SEM micrographs of the resulting anodic aluminum oxide (AAO), showing the internal pore geometries at the early, middle, and last stage of anodization, respectively. The white arrow in (b) indicates the oxide interface formed by the transition from the first-step anodization at 140 V to the second one at 160 V.

of anodization is characterized as symmetric sinusoidal oscillations with $j_{Min} > 0.1$ A cm^{-2}, while asymmetric ones with $j_{Min} > 0.01$ A cm^{-2} for the later stage. These three characteristics were commonly observed also from the second-step HA performed at other voltages (e.g., $U_2 = 140$ V, 180 V, and 200 V; see Supporting Information, Fig. S2).

Figure 1b–d presents the internal morphologies of pores, which correspond to the early, middle, and last stage of the second-step HA at 160V in Figure 1a, respectively. It is clear from Figure 1b that the change of anodization condition from the first-step HA to the second-step one results in a marked transition of the pore geometry along the pore axes, as indicated by a white arrow (i.e., transition from uniform pore diameters to modulated ones). It is noteworthy here that the direction of pores was observed to be straight without branching or dying in spite of the change in anodization potential from $U_1 = 140$ V to $U_2 = 160$ V. The cross-section scanning electron microscopy (SEM) images of the anodic alumina well reflect the observed oscillatory kinetic behavior shown in Figure 1a. The period of diameter modulations increases with the anodization time, consistent with the observed current–time transient. We found that there is a one-to-one correlation

between the internal pore geometry and each current peak profile in the *j*–*t* curve. Pores formed at the early stage of anodization are characterized as symmetrical geometry along the pore axes (Fig. 1b), while pores for the later stage as asymmetrical one (Fig. 1c). We observed solidified gel-like material at the bottom part of an as-prepared AAO (~1.5 μm from the barrier layer), which partly blocks pores and thus prevents clear examination of the internal pore structure (Fig. 1d). This gel-like material turned out to be very soluble in 5 wt% H_3PO_4 or 0.3 M $H_2C_2O_4$ at room temperature.

The observed structural evolution of the pores during the second-step HA can be attributed to the spontaneous current oscillations, of which the maximum amplitude is as large as ~0.7 A cm^{-2}. Figure 2 illustrates how the details of oscillatory anodization kinetics affect the internal pore geometry of AAO; symmetrically modulated pores for symmetric sinusoidal current oscillations (Fig. 2c and d) and ratchet-type asymmetric pores for asymmetric current oscillations (Fig. 2e and f). We found that the pore diameter (D_p) increases with the current density (j) at a given potential (U_2).

As we mentioned earlier, the current in anodization of aluminum is related to the passage of ionic species through the barrier layer. Under high field conditions, the ionic current density (j) can be related to the electric field strength (E) through the following exponential law;[32,33]

$$j = j_o \exp(\beta E) = j_o \exp(\beta \Delta U / t_b) \quad (1)$$

where j_o and β are material-dependent constants and $\Delta U/t_b$ is the effective electric field strength (E) across the barrier layer of thickness t_b. Accordingly, one would expect from the high-field conduction theory that the thickness of barrier layer (t_b) be inversely proportional to the logarithm of current density (j) at a given anodization potential. In order to see the effect of current density (j) on the structure of the barrier layer, we have performed microscopic investigations to compare the morphologies of oxide nanopores that were prepared from two separate anodization experiments, whose reactions were terminated near j_{Min} and j_{Max} in oscillating currents. Figure 3a and b present barrier layer structures of AAOs prepared by stopping the second-step HA reactions ($U_2 = 200$ V) at a low ($j = 0.086$ A cm^{-2}) and high current density ($j = 0.881$ A cm^{-2}), respectively (see Fig. S3 of the Supporting Information for the corresponding *j*–*t* curves). A schematic cross-section of AAO on aluminum and the parameters defining the geometry of the barrier layer are shown in Figure 3c and the table in Figure 3d, respectively. It turned out from our statistical analysis that the thickness of the barrier layer ($t_b^{at\ high\ j}$) formed at a high current density is only slightly smaller than that ($t_b^{at\ low\ j}$) at a low current density with $t_b^{at\ low\ j}/t_b^{at\ high\ j} \approx 1.04$ (see the table in Fig. 3). In fact, high-field conduction theory predicts that a small difference of the barrier-layer thickness will result in a large difference in current density. For an anodic film of aluminum with the pre-exponential factor $j_o \approx 10^{-18}$ A cm^{-2} in Equation 1,[33,34] theory predicts $t_b^{at\ low\ j}/t_b^{at\ high\ j} \approx 1.06$. On the other hand, upon close examination of the SEM images in Figure 3a and b, we found that the detailed shapes of the electrolyte/oxide (e/o) and oxide/metal (o/m) interfaces are different. The curvature radius ($R = a/\sin\theta$) of the o/m interface was observed to be larger for AAO formed at a high j compared to that at a low j (i.e., $\theta^{\text{ at low } j} > \theta^{\text{ at high } j}$). We assume that at a given potential the electric field and the current distributions in the

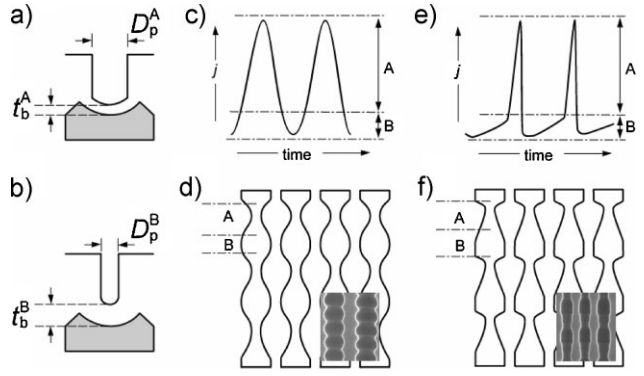

Figure 2. Schematics illustrating the effect of current oscillations on the pore morphology of the resulting anodic aluminum oxide (AAO). a,b) the cross-sections of AAO structures formed at high and low current density (j) region, respectively; t_b = the thickness of the barrier layer, D_p = the pore diameter. The superscripts A and B in t_b and D_p denote that each quantity corresponds to that of high and low current density, respectively. c,d) Current–time transients with symmetric oscillations and the internal pore geometry of the resulting AAO, respectively. e,f) Current–time transients with asymmetric oscillations and the internal pore geometry of the resulting AAO, respectively. The parts marked as the capital A and B in the panel (d) and (f) correspond to the oxide segments formed at high and low current density (j) regions that are marked as A and B in the panel (c) and (e), respectively. Representative cross-sectional SEM micrographs of AAOs which have experienced symmetric and asymmetric current oscillations are shown as insets in (d) and (f), respectively.

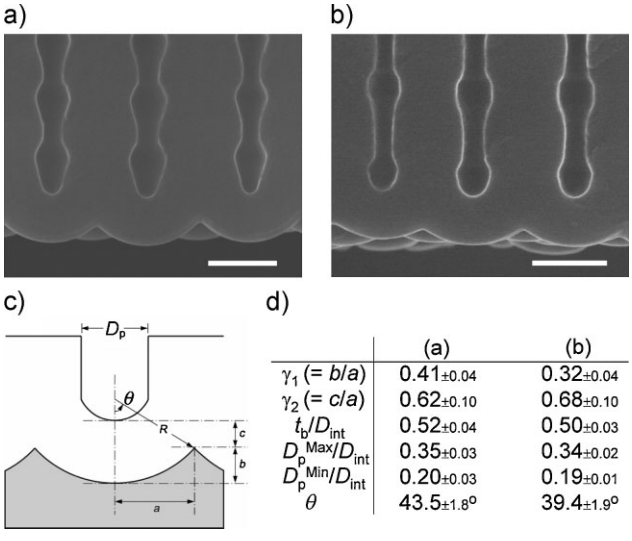

	(a)	(b)
γ_1 (= b/a)	0.41±0.04	0.32±0.04
γ_2 (= c/a)	0.62±0.10	0.68±0.10
t_b/D_{int}	0.52±0.04	0.50±0.03
D_p^{Max}/D_{int}	0.35±0.03	0.34±0.02
D_p^{Min}/D_{int}	0.20±0.03	0.19±0.01
θ	43.5±1.8°	39.4±1.9°

Figure 3. a,b) Cross-section FE-SEM micrographs of AAOs prepared from two separate anodization experiments ($U_2 = 200$ V), whose reaction were terminated near j_{Min} and j_{Max} in oscillating currents; a) $j = 0.086$ A cm^{-2}, b) $j = 0.881$ A cm^{-2}. c) A schematic cross-section of AAO on aluminum substrate. d) The parameters defining the geometry of the barrier layer shown in (c); D_p = the pore diameter, $D_{int} = 2a$ = the interpore distance, $t_b = b + c$ = the thickness of the barrier layer, R = the radius of curvature, $\theta = \cos^{-1}[1 - 2b^2/(a^2 + b^2)]$. Scale bars in (a) and (b) = 250 nm.

barrier oxide might sensitively be varied with the detailed geometry of the barrier layer, which will govern not only the local rates of motion of the e/o and o/m interfaces, and hence the porosity of the oxide (i.e., pore diameter, D_p), but also the evolution of mechanical stresses. The observed evolution of the radius (R) of curvature of the o/m interfaces can be attributed to the different ellipticities of the e/o interfaces for both samples. For low current density, we expect that the speed of motion of the o/m interface on the ridge is retarded to a larger extent compared to the interface speed in the scalloped region due to the large ellipticity of the e/o interface (see Fig. 3a), resulting in greater recession of the o/m interface at the scalloped region compared to the case of high current density (i.e., $\gamma_1^{\text{at low } j} > \gamma_1^{\text{at high } j}$ in Fig. 3d). This argument is in line with recent theoretical studies by Houser et al., who have shown that the receding rate of the o/m interface both at the scalloped region and the ridge sensitively varies with the elliptic e/o interface profile, and predicted the pseudoconvective motion of mobile anions (i.e., oxide materials) from the pore center towards the cell boundary,[35,36] which accounts for both recession of the e/o interface at the pore base and also accumulation of oxide at the pore wall,[37,38] unlike previous models based on field-assisted chemical dissolution of oxide.[31,39–41]

3.2. The Origin of Spontaneous Current Oscillations

Previously, Taveira et al. observed large irregular voltage oscillations during anodization of titanium under specific galvanostatic conditions.[29] Based on morphological investigations of the samples, they suggested that the voltage oscillations are triggered by the undermining of the regular porous oxide layer by a less-ordered porous layer, and accompanied by successive detachments of porous TiO_2 layers from the metal (i.e., Ti), which lead to voltage drops due to an easy electrolyte access to the metal surface. The voltage oscillations are suggested to be maintained by a competition of conditions forming typical porous oxide and conditions forming a disordered porous layer. The observed morphological evolution and the mechanism responsible for lift-off of the growing anodic TiO_2 films are very much similar to the case of galvanostatic anodization of silicon, in which spontaneous regular oscillations of voltage are associated with sequential growth of the oxide films and a subsequent detachment of these films by local dissolution of oxide at the oxide/silicon interface.[22–25,28] In other words, oscillatory kinetic behaviors during the anodization of titanium or silicon have been attributed to a cyclic process of growth and detachment of anodic oxides forming a stack of oxide layers. If we assume that a similar process takes place during the second-step HA of the present work, the formation of a stack of AAO would be expected as a result of spontaneous current oscillations. However, we could not observe delamination of anodic oxide layer from the anode surface. We were able to obtain AAO samples in the form of a single piece of rigid free-standing film, implying that the origin of the spontaneous current oscillations during anodization of aluminum might be different from the cases of titanium or silicon anodizations.

In the present study we could observe spontaneous current oscillations only during the second-step HA, although the triggering of oscillations could not always be observed. Repeated experiments indicated that the oscillatory behavior takes place for about 90% of the experiments and its probability of occurring increases with the anodization potential (U_2). The differences of electrochemical conditions for the first- and the second-step HA are the electrolyte stirring, anodizing voltage, and temperature of the aluminum substrate. Among them, electrolyte stirring and temperature of the aluminum substrate are thought to be the main factors triggering current oscillations considering the fact that the oscillatory behavior can occur even at $U_1 = U_2 = 140$ V, although there is an induction time until current oscillations occur (see Supporting Information, Fig. S2a).

In order to gain more insight into the origin of spontaneous current oscillations during the second-step anodization, the effect of electrolyte stirring was investigated by monitoring current-time transient while the stirring of the electrolyte is stopped and then restarted. The current-time transient in Figure 4 shows the effect of electrolyte stirring on the current oscillations during the second-step HA at 180 V. Current oscillations disappeared when stirring of the electrolyte was started and then appeared again when stirring was stopped. The experimental observation reveals undoubtedly that oscillatory behavior is related to the diffusion of the electrolyte from the bulk reservoir to the bottom of the nanopores. We propose that diffusion-controlled electrochemical oxidation of aluminum is mainly responsible for the current oscillations during the second-step HA. Under an unstirred condition the following consecutive events could concurrently take place in every pore: Oxidation of aluminum under an HA condition will quickly deplete oxygen-containing anionic species at the bottom of pores accompanying with a large increase in ionic current, and establish a large concentration gradient of anions along the narrow pore channels. Depletion of anions at the pore bottom will in turn result in retardation of the anodic oxidation reaction and thus to a decrease in current density. At this stage a new cycle will begin by the influx of anions due to the vertical diffusion of electrolyte from the bulk reservoir to the reaction interface at the bottom of pores. We believe that in each oscillation the concentration difference at

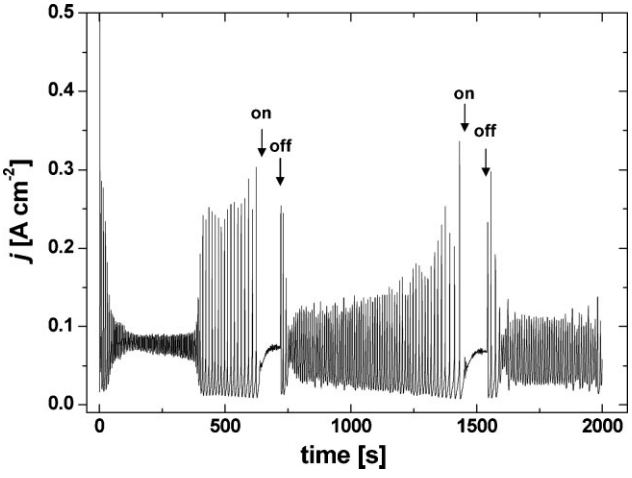

Figure 4. Current–time transient showing the effect of electrolyte stirring on the current oscillations during the second-step HA at 180 V.

the pore mouth and pore bottom is proportional to the diffusion length of anions (i.e., the length of pores) and/or to the peak current (j) of the previous oscillation, which would explain symmetric current oscillations with short periods at the early stage of HA and asymmetric current oscillations with longer periods at the later stage (see Fig. 1). On the other hand, electrolyte stirring will furnish a condition of continuous supply of fresh electrolyte to the reaction interface, perturbing the concentration gradient established along the pore channels.

Figure 5 shows the effect of an instant agitation of the electrolyte on the current oscillations and the internal morphology of pores. It is immediately apparent from the current–time curve in Figure 5a that an instant electrolyte agitation triggers irregular current oscillations, revealing perturbation of the concentration gradient established along the pores. The present experiment further supports our assumption that diffusion-controlled oxidation reaction is mainly responsible for the current oscillations during the second-step HA. From Figure 5c, it is readily evident that oscillation profiles of the current are well reflected in the internal morphology of pores. The AAO sample exhibits high degree of directional coherency of pores as shown in Figure 5b.

3.3. Local Heat Development

For the second-step HA, we observed that the central region of an AAO sample exhibits a slightly different color than the surrounding area (i.e., light brown color at the center and bright yellow at the surrounding). For AAO samples anodized for an extended period of time, we could observe a distinct spot with dark brown color at the center. We found that there is a thickness distribution over the AAO film. Oxide thickness at the central region turned out to be thicker than that at the surrounding area. Figure 6 shows a representative cross-sectional SEM image of a long-term anodized AAO at 160 V. The specimen for SEM investigation was taken from the central area of the sample. Pores at the upper part of the sample are straight, but distorted at the lower part. Microscopic undulations are observed from the bottom side of the AAO, revealing plastic deformation of the aluminum substrate during anodization. Pore diameters of AAO appear to be larger at the upper part compared to at the bottom part. Local oxide thickening at the central area and the morphological evolutions of long-term anodized AAO can be explained by considering the local heat development and the convection flow of electrolyte during anodization of aluminum with an unstirred electrolyte solution.

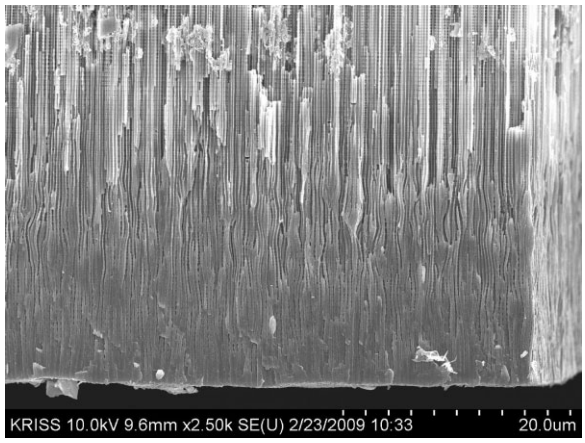

Figure 6. Cross-sectional SEM micrograph of anodic aluminum oxide (AAO) that experienced large thermal and mechanical stress at the oxide/metal interface.

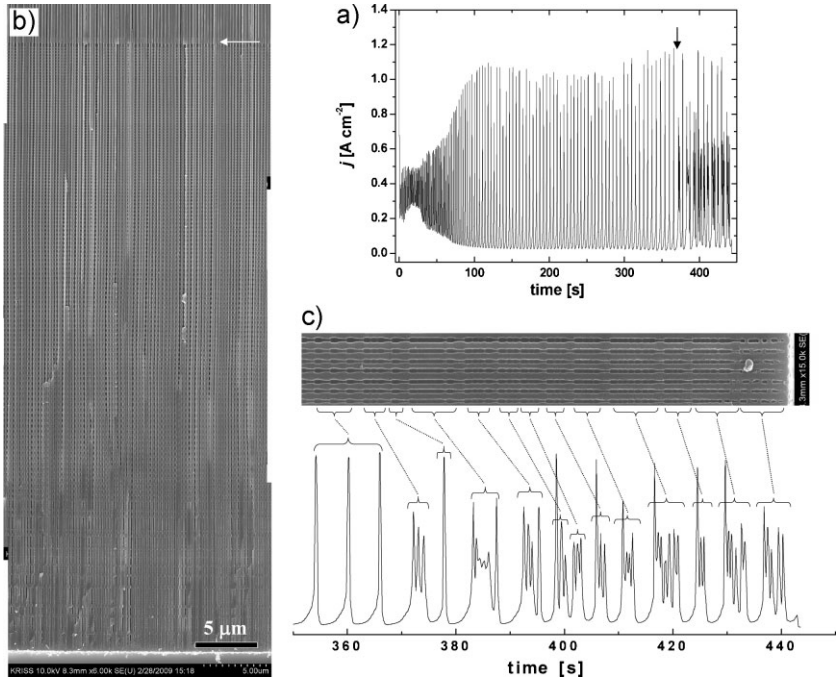

Figure 5. The effect of an instant agitation of the electrolyte on a) the current oscillations and b) the internal morphology of pores. An instant solution agitation was introduced at the time indicated by the arrow in (a). The white arrow in (b) indicates the oxide interface formed by the transition from the fist-step anodization at 180 V to the second step at 200 V. An enlarged current-time curve after the electrolyte agitation is shown in (c), together with the corresponding pore structure of AAO.

The reaction involved in anodic oxidation of aluminum is exothermic. Previous studies have shown that the rise in temperature can be several tens of degrees centigrade at high current densities (e.g., $\Delta T \approx 60^{\circ}\mathrm{C}$ at $j \approx 0.3\ \mathrm{A\ cm^{-2}}$).[42,43] The main contribution to heat generation in anodization of aluminum is related to current flow through the barrier oxide layer. The production of Joule's heat (Q) for a given time t is proportional to the square of the current density (j) according to the following equation;

$$Q = \Delta U j t = R_b j^2 t \qquad (2)$$

where ΔU and R_b are the potential drop across the barrier layer and the resistance of the

barrier layer, respectively. The maximum current (j_{Max}) during the current oscillations in the second-step HA is roughly two orders of magnitude higher than the current in conventional mild anodizations (MA). Accordingly, spontaneous current oscillations during the second-step HA are accompanied by periodic evolutions of large reaction heat. At the early stage of the second-step HA Joule's heat can be dissipated through both the electrolyte initially at 5 °C and the cooling plate just underneath the anode. However, anodization for an extended period of time gradually increases the temperature of the bulk electrolyte, which we believe is the primary reason for pore widening by acidic dissolution of oxide at the upper part of AAO. Joule's heat from the anode is believed to be transferred to the bulk electrolyte through a naturally developing convective flow of the electrolyte. Considering the geometry of the electrochemical setup used in the present work, we can expect a similar convective motion of an electrolyte that occurs in a wall-jet electrode reactor at zero jet condition, in which the initially stagnant electrolyte, adjacent to the anode surface, heats up by the anodic reaction and moves upward in the cell, eventually creating a natural flow pattern with fresh electrolyte being drawn in from the rim of the anode.[39,40,44] For anodization in a wall-jet electrode reactor, it was reported that the temperature is highest at the center of the anode where the local convection transfer coefficient is highest, and it decrease gradually in the radial direction due to the natural convection flow of the electrolyte.[40] In analogy, we believe that a local temperature distribution established along the anode surface results in a non-uniform current flow and thus non-uniform thickness distribution of the anodic film. In other words, the thicker oxide at the central area of AAO compared to the surrounding region can be attributed to greater local current that is associated with local temperature rise. The electrochemical event at the central area of anode and the evolution of distorted pore channels at the lower part of AAO in Figure 6 are a reminiscence of local breakdown process of anodic oxide under localized flow of high current. Anodic oxidation of aluminum is a volume expansion process, and thus accompanied by compressive stress along the metal/oxide film interface which was found to play a role in the self-ordering of oxide nanopores.[45,46] Since volume expansion factor is proportional to the current density j,[15,47,48] a very high level of stress can be expected during large oscillations of current. We believe that a consequence of non-uniform intense mechanical stresses at the metal/oxide interface is plastic deformation of aluminum substrate and the observed distorted pore channels in the anodic oxide film.

3. Conclusions

In summary, nanoporous anodic aluminum oxide (AAO) has been prepared by hard anodization (HA) of aluminum under potentiostatic conditions using 0.3 M $H_2C_2O_4$. Under unstirred electrolyte condition, spontaneous current oscillations could be observed. The amplitude and period of current oscillations were observed to be increased with anodization time. As a consequence of oscillatory kinetic behavior, anodic alumina exhibited modulated pore structures, in which the diameter contrast and the length of pore modulation increase with the amplitude and the period of current oscillations, respectively, and the current peak profile determines the internal geometry of oxide nanopores. The mechanism responsible for the oscillatory behavior is assumed to be a diffusion-controlled anodic oxidation of aluminum. In the case of long-term anodized samples, anodic alumina films exhibit non-uniform thickness distributions and undesired pore structures at the bottom part of film. The observed local oxide thickening at the central area and distorted pores at the bottom part of long-term anodized AAOs were explained in terms of local heat development under unstirred electrolyte condition and non-uniform distribution of large mechanical stress that is associated with high current density. The present study reveals that one may achieve structural engineering of nanoporous AAO by deliberately manipulating the current during a potentiostatic anodization of aluminum. Apart from template applications for developing low-dimensional nanostructures, we expect that AAO membranes with modulated pore structure could be starting materials for developing three-dimensional porous architectures that may have potential for photonic applications, and model systems for investigating separations of particles and adsorption characteristics of molecules. In fact, we were able to fabricate an AAO membrane with a novel three-dimensional porous architecture by extended etching of pores by phosphoric acid solution (see Fig. 7).

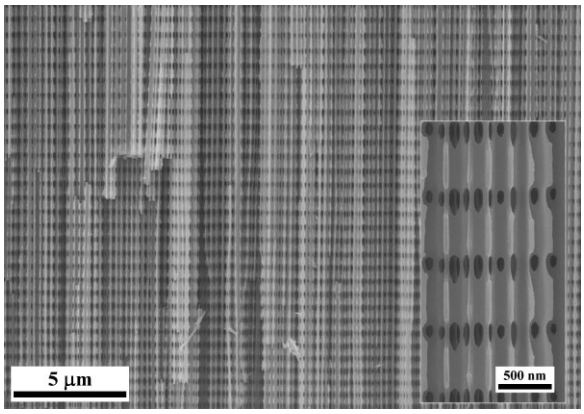

Figure 7. SEM micrograph of anodic aluminum oxide (AAO) with three-dimensional porous architecture. The inset shows an enlarged SEM image. The second-step anodization was performed at $U_2 = 140$ V. After anodization, pore widening was carried out by using 5 wt% H_3PO_4 (30 °C).

4. Experimental

Aluminum Pre-Treatment: As-received aluminum disks of 2 cm in diameter (Goodfellow, 99.999%) were used in anodization experiments without the annealing step. The aluminum disks were electrochemically polished in an 1:4 mixture solution of 65% $HClO_4$, and 99.5% ethanol (5 °C) in order to exclude, if any, potential side effect (e.g., localized field concentration) that could arise from the surface roughness during anodization.

Anodization of Aluminum: A mirror-finished aluminum disk was placed in an electrochemical cell with an O-ring, so that one side of metal can be anodized. The area exposed to the electrolyte solution was 1.96 cm^2. All anodization experiments in the present work were performed by using an electrochemical cell equipped with a cooling stage that is in thermal contact with the aluminum substrate to remove the reaction heat. Direct thermal contact between the aluminum substrate and the cooling stage provides an

efficient way for dissipating the reaction heat liberated during oxide growth. The experimental procedure employed in the present study comprises two consecutive hard anodizations (HA) using 0.3 M oxalic acid as an electrolyte under different electrochemical conditions (i.e., voltage (U), temperature, and solution stirring). The first-step HA was conducted at $U_1 = 140$ V, 160 V, or 180 V with a vigorously stirred electrolyte at 0 °C for 20 min according to the method reported previously [14]. The resulting anodic film exhibited a bright golden color. Afterwards, the second-step HA was carried out at voltage ranging from $U_2 = 140$ V to 200 V at an elevated temperature (5 °C) without stirring of the electrolyte. Limiting current density of the power supply was set at 0.51–1.53 A cm^{-2}. Current densities (j) reported in this paper were calculated by dividing the measured values of current (I) by the anodized sample area, not by the effective surface area considering the detailed hemispherical geometry of the barrier layer.

Microscopic Characterization: After anodization, the remaining aluminum substrate was removed by using a mixture solution of $CuCl_2$ and HCl. A Hitachi S-4800 field emission scanning electron microscope (FE-SEM) was employed for the morphological characterization of the resulting anodic film. SEM cross-sectional investigations were carried out on mechanically broken samples.

Acknowledgements

This work is supported by Korea Research Council of Fundamental Science and Technology (KRCF) through the KRISS project of ''Development of Advanced Industrial Metrology''. Supporting Information is available online from Wiley InterScience or from the author.

Received: July 6, 2009
Published online: October 8, 2009

[1] S. Wernick, R. Pinner, P. G. Sheasby, *The Surface Treatment and Finishing of Aluminum and Its Alloys*, 5th ed., Vol. *1*, Finishing Publications & ASM International, Ohio **1996**.
[2] F. Keller, M. S. Hunter, D. L. Robinson, *J. Electrochem. Soc.* **1953**, *100*, 411.
[3] H. Masuda, K. Fukuda, *Science* **1995**, *268*, 1466.
[4] W. Lee, R. Ji, C. A. Ross, U. Gösele, K. Nielsch, *Small* **2006**, *2*, 978.
[5] S. R. Nicewarner-Peña, R. G. Freeman, B. D. Reiss, L. He, D. J. Peña, I. D. Walton, R. Cromer, C. D. Keating, M. J. Natan, *Science* **2001**, *294*, 137.
[6] S. B. Lee, D. T. Mitchell, L. Trofin, T. K. Nevanen, H. Söderlund, C. R. Martin, *Science* **2002**, *296*, 2198.
[7] L. Qin, S. Park, L. Huang, C. A. Mirkin, *Science* **2005**, *309*, 113.
[8] L. Liu, W. Lee, R. Scholz, E. Pippel, U. Gösele, *Angew. Chem. Int. Ed.* **2008**, *47*, 7004.
[9] W. Lee, H. Han, A. Lotnyk, M. A. Schubert, S. Senz, M. Alexe, D. Hesse, S. Baik, U. Gösele, *Nat. Nanotechnol.* **2008**, *3*, 402.
[10] Z. Huang, X. Zhang, M. Reiche, L. Liu, W. Lee, T. Shimizu, S. Senz, U. Gösele, *Nano Lett.* **2008**, *8*, 3046.
[11] L. Bruschi, G. Fois, G. Mistura, K. Skarek, R. Hillebrand, M. Steinhart, U. Gösele, *Langmuir* **2008**, *24*, 10936.
[12] F. Casanova, C. E. Chiang, C.-P. Li, I. V. Roshchin, A. M. Ruminski, M. J. Sailor, I. K. Schuller, *Nanotechnology* **2008**, *19*, 315709.
[13] S. Matthias, F. Müller, *Nature* **2003**, *424*, 53.
[14] W. Lee, R. Ji, U. Gösele, K. Nielsch, *Nat. Mater.* **2006**, *5*, 741.
[15] W. Lee, K. Schwirn, M. Steinhart, E. Pippel, R. Scholz, U. Gösele, *Nat. Nanotechnol.* **2008**, *3*, 234.
[16] W. Lee, R. Scholz, U. Gösele, *Nano Lett.* **2008**, *8*, 2155.
[17] D. Losic, M. Lillo, D. Losic, Jr, *Small* **2009**, *5*, 1392.
[18] K. Schwirn, W. Lee, R. Hillebrand, M. Steinhart, K. Nielsch, U. Gösele, *ACS Nano* **2008**, *2*, 302.
[19] R. L. Van Meirheghe, F. Cardon, W. P. Gomes, *Electrochim. Acta* **1979**, *24*, 1047.
[20] J. Garstensen, R. Prange, G. S. Popkirov, H. Föll, *Appl. Phys. A* **1998**, *67*, 459.
[21] J. Carstensen, R. Prange, H. Föll, *J. Electrochem. Soc.* **1999**, *146*, 1134.
[22] V. P. Parkhutik, E. Matveeva, *Electrochem. Solid-State Lett.* **1999**, *2*, 371.
[23] V. Parkhutik, E. Matveeva, R. Perez, J. Alamo, D. Betrán, *Mater. Sci. Eng. B* **2000**, *69–70*, 553.
[24] V. Parkhutik, *Electrochim. Acta* **2000**, *45*, 3249.
[25] V. Parkhutik, *Solid-State Electron.* **2001**, *45*, 1451.
[26] S. Langa, J. Carstensen, I. Tiginyanu, M. Christophersen, H. Föll, *Electrochem. Solid-State Lett.* **2001**, *4*, G50.
[27] E. Harvey, D. N. Buckley, S. N. G. Chu, *Electrochem. Solid-State Lett.* **2002**, *5*, G22.
[28] V. Parkhutik, J. Curiel-Esparza, M.-C. Millan, J. Albella, *Phys. Status Solidi A* **2005**, *202*, 1576.
[29] L. V. Taveira, J. M. Macak, K. Sirotna, L. F. P. Dick, P. Schmuki, *J. Electrochem. Soc.* **2006**, *153*, B137.
[30] W. Lee, K. Nielsch, U. Gösele, *Nanotechnology* **2007**, *18*, 475713.
[31] F. Li, L. Zhang, R. M. Metzger, *Chem. Mater.* **1998**, *10*, 2470.
[32] A. Güntherschulze, H. Betz, *Z. Phys.* **1934**, *92*, 367.
[33] M. M. Lohrengel, *Mater. Sci. Eng. R* **1993**, *11*, 243.
[34] W. Mizushima, *J. Electrochem. Soc.* **1961**, *108*, 825.
[35] J. E. Houser, K. R. Hebert, *J. Electrochem. Soc.* **2006**, *153*, B566.
[36] J. E. Houser, K. R. Hebert, *Nat. Mater.* **2009**, *8*, 415.
[37] S. J. Garcia-Vergara, P. Skeldon, G. E. Thompson, H. Habazaki, *Electrochim. Acta* **2006**, *52*, 681.
[38] P. Skeldon, G. E. Thompson, S. J. Garcia-Vergara, L. Iglesias-Rubianes, C. E. Blanco-Pinzon, *Electrochem. Solid-State Lett.* **2006**, *9*, B47.
[39] I. De Graeve, H. Terryn, G. E. Thompson, *J. Appl. Electrochem.* **2002**, *32*, 73.
[40] I. De Graeve, H. Terryn, G. E. Thompson, *J. Electrochem. Soc.* **2003**, *150*, B158.
[41] J. P. O'Sullivan, G. C. Wood, *Proc. R. Soc. London Ser. A* **1970**, *317*, 511.
[42] F. R. Applewhite, J. S. L. Leach, P. Neufeld, *Corros. Sci.* **1969**, *9*, 305.
[43] L. E. Fratila-Apachitei, I. DeGraeve, I. Apachitei, H. Terryn, J. Duszczyk, *Surf. Coat. Technol.* **2006**, *200*, 5343.
[44] L. E. Fratila-Apachitei, I. D. Graeve, I. Apachitei, H. Terryn, J. Duszczyk, *Surf. Coat. Technol.* **2006**, *200*, 5343.
[45] A. P. Li, F. Müller, A. Birner, K. Nielsch, U. Gösele, *J. Appl. Phys.* **1998**, *84*, 6023.
[46] O. Jessensky, F. Müller, U. Gösele, *Appl. Phys. Lett.* **1998**, *72*, 1173.
[47] I. Vrublevsky, V. Parkoun, J. Schreckenbach, G. Marx, *Appl. Surf. Sci.* **2003**, *220*, 51.
[48] I. Vrublevsky, V. Parkoun, V. Sokol, J. Schreckenbach, G. Marx, *Appl. Surf. Sci.* **2004**, *222*, 215.